Journal of
Computational and Theoretical Nanoscience
Vol. 7, 2441–2447, 2010

Quantum Machine Using Cold Atoms

Alexey V. Ponomarev[1,*], Sergey Denisov[1], and Peter Hänggi[1,2]

[1] *Institute of Physics, University of Augsburg, Universitätstr. 1, D-86159 Augsburg*
[2] *Department of Physics and Center for Computational Science and Engineering, National University of Singapore, 117542, Singapore*

For a machine to be useful in practice, it preferably has to meet two requirements: namely, (i) to be able to perform work under a load and (ii) its operational regime should ideally not depend on the time at which the machine is switched-on. We devise a minimal setup, consisting of two atoms only, for an ac-driven quantum motor which fulfills both these conditions. Explicitly, the motor consists of two different interacting atoms placed into a ring-shaped periodic optical potential—an optical "bracelet,"—resulting from the interference of two counter-propagating Laguerre-Gauss laser beams. This bracelet is additionally threaded by a pulsating magnetic flux. While the first atom plays a role of a quantum "carrier," the second serves as a quantum "starter," which sets off the "carrier" into a steady rotational motion. For fixed zero-momentum initial conditions the asymptotic carrier velocity saturates to a unique, nonzero value which becomes increasingly independent on the starting time with increasing "bracelet"-size. We identify the quantum mechanisms of rectification and demonstrate that our quantum motor is able to perform useful work.

Keywords: Transport Processes, Atoms in Optical Lattices, Electric Motors.

1. INTRODUCTION

The development of laser cooling techniques and the creation of the Bose-Einstein condensates (BEC) present landmark successes of modern experimental physics.[1] Since 1995,[2] ultracold atoms rapidly become a popular toolbox to explore the quantum world. Subsequent experimental studies can be (conditionally) divided into three stages. The first one was aimed to model the electronic behavior in solids with ultracold atoms trapped in periodic optical potentials. These potentials, so called optical lattices thus implement the idea of "quantum simulators," proposed by Feynman in 1982.[3] Incarnation of paradigmatic quantum models (Bose- and Fermi-Hubbard systems, Tonk-Girardeau gas and etc.)[4] and their intensive experimental studies mark the second stage. The recent advent of a third wave, namely "to make use of it," triggered a search for applications which led to single atom qubits,[5] atom optical clocks,[6] cold atom interferometry,[7] as well as cold atom gyroscopes.[8]

An electric motor, i.e., a device that converts electrical energy into mechanical work by setting a working body into a linear or rotational motion, is a archetype example of a useful physical system. For nearly two centuries, since the invention of the first electrical motor,[9] a never-ending continuous miniaturization has already passed the microscale level[10] and entered the nano-scale world.[11] Yet, this process alone does not parallel the transition from the classical to the quantum world: the operational descriptions of all existing electrical, nano-sized motors rest on classical concepts.[11]

With this present work, we provide a detailed analysis for an electric *quantum* motor proposed recently in Ref. [12]. This motor is made of two ultracold atoms only that are trapped in a deep ring-shaped one-dimensional optical lattice,—an optical "bracelet." The blueprint for such an underlying trapping potential was proposed recently[13] and a first experimental realization has been reported in Ref. [14]. We employ this setup to devise an engine which works as a genuine ac-driven quantum motor. We identify the quantum mechanisms which yield the *modus operandi* for a motor device. Moreover, we discuss parameter values suitable for the realization of the quantum engine with present-day experimental setups.

2. THE MOTOR SETUP

Figure 1 is a sketch of our quantum machine device. The optical potential, which results either from the interference of a Laguerre-Gauss (LG) laser beam with a plane wave[13] or, alternatively, of two collinear LG beams with different frequencies[14] is capable of trapping two interacting atoms. The first atom, termed "carrier," c, is assumed to be charged and is driven by the time-dependent magnetic flux

*Author to whom correspondence should be addressed.

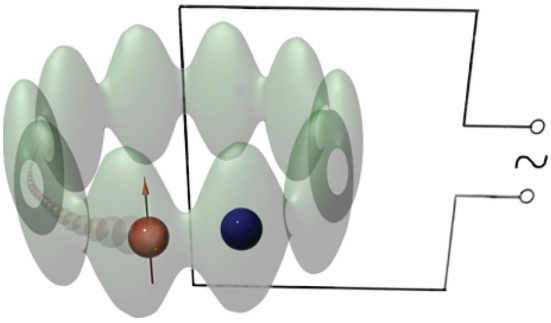

Fig. 1. Sketch of the quantum machine: Two ultracold atoms are loaded into an optical "bracelet"—a ring-shaped optical lattice. Both atoms interact locally with each other, while only one carrier (the one with an arrow) is magnetically driven.

piercing the bracelet.[15] The second atom, termed "starter," s, is neutral thus remains unaffected by the magnetic flux, but interacts locally, e.g., by means of atom-s-wave scattering, with the carrier when both atoms share the same site of the optical lattice.

We next assume that both atoms are loaded into the lowest energy band of a deep, ring-shaped optical potential with L lattice sites with the lattice constant d. The time-dependent homogeneous vector potential $\tilde{A}(t)$ does not induce any appreciable transitions between the ground band and the far separated excited band(s).

The total Hamiltonian of the system reads

$$H_{\mathrm{tot}} = H_{\mathrm{c}}(t) + H_{\mathrm{s}} + H_{\mathrm{int}} \tag{1}$$

where the time-dependent Hamiltonian H_{c} for the carrier is given by

$$H_{\mathrm{c}}(t) = -\frac{J_{\mathrm{c}}}{2}\left(\sum_{l_{\mathrm{c}}=1}^{L} e^{i\tilde{A}(t)}|l_{\mathrm{c}}+1\rangle\langle l_{\mathrm{c}}| + \mathrm{H.c.}\right)\otimes \mathbf{1}_{\mathrm{s}} \tag{2}$$

and the starter Hamiltonian H_{s} reads

$$H_{\mathrm{s}} = -\frac{J_{\mathrm{s}}}{2}\left(\sum_{l_{\mathrm{s}}=1}^{L} |l_{\mathrm{s}}+1\rangle\langle l_{\mathrm{s}}| + \mathrm{H.c.}\right)\otimes \mathbf{1}_{\mathrm{c}} \tag{3}$$

Here, J_{c} and J_{s} are the corresponding hopping strengths to neigbouring sites, which depend on the atom mass, M, and the potential depth, V_0. Here, for both atoms, we have assumed the limit of a deep periodic potential, also refereed to as the tight-binding model. This limit is well justified for a potential amplitudes of $V_0 \gtrsim 5E_0$, where the higher-order tunneling amplitude is less than 10% of the leading first-order (i.e., the next neighbour) tunneling amplitude.[4] $E_0 = \hbar^2\pi^2/2Md^2$ is the "recoil" energy. The salient carrier-starter on-site interaction is

$$H_{\mathrm{int}} = W\sum_{l_{\mathrm{c}},\, l_{\mathrm{s}}=1}^{L} \delta_{l_{\mathrm{c}},\, l_{\mathrm{s}}}|l_{\mathrm{c}}\rangle\langle l_{\mathrm{c}}|\otimes|l_{\mathrm{s}}\rangle\langle l_{\mathrm{s}}| \tag{4}$$

where W denotes the interaction strength. Throughout the remaining, we use periodic boundary conditions; i.e., $|L+1\rangle = |1\rangle$. The dimension of the complete Hilbert space is $\mathcal{N} = L^2$. The total system is described by wave function $|\psi(t)\rangle$. The scale of the motor current will be measured in units of the maximal group velocity $v_0 = J_{\mathrm{c}}d/\hbar$.

To conclude with the setup, we specify that the driving is switched on at the time t_0, so that the vector potential has the form

$$\tilde{A}(t;t_0) = \chi(t-t_0)A(t) \tag{5}$$

where $\chi(t-t_0)$ is the step function, and $A(t)$ is defined on the entire time axis, $t\in(-\infty,+\infty)$.

3. DC-QUANTUM CURRENT

The mean carrier current is given as the speed of the motor by means of the velocity operator: $\hat{v}_{\mathrm{c}}(t;t_0) = i/\hbar[H_{\mathrm{tot}}(t),\hat{x}_{\mathrm{c}}]$. With $\hat{x}_{\mathrm{c}} = d\sum_l l_{\mathrm{c}}|l_{\mathrm{c}}\rangle\langle l_{\mathrm{c}}|\otimes\mathbf{1}_{\mathrm{s}}$, one finds $\hat{v}_{\mathrm{c}}(t;t_0) = -i(v_0/2)(\sum_{l_{\mathrm{c}}=1}^{L} e^{i\tilde{A}(t;t_0)}|l_{\mathrm{c}}+1\rangle\langle l_{\mathrm{c}}| - \mathrm{H.c.})\otimes\mathbf{1}_{\mathrm{s}}$. In the quasimomentum representation with $|\kappa_l\rangle = \sum_{n=1}^{L}\exp(i\kappa_l n)|n\rangle$, its quantum expectation $v_{\mathrm{c}}(t;t_0) = \langle\psi(t)|\hat{v}_{\mathrm{c}}(t;t_0)|\psi(t)\rangle$ reads

$$v_{\mathrm{c}}(t;t_0) = v_0\sum_{l=1}^{L}\rho_{\kappa_l}(t;t_0)\sin(\kappa_l + \tilde{A}(t;t_0)) \tag{6}$$

wherein $\kappa_l = 2\pi l/L$ is the single particle quasimomentum and where we indicated explicitly the parametric dependence on the start time t_0. Further, $\rho_\kappa(t;t_0) = \sum_{l_{\mathrm{s}}}|\langle\psi(t)|\kappa_{l_{\mathrm{s}}},\kappa_{l_{\mathrm{c}}}\rangle|^2$, where $|\kappa_{l_{\mathrm{s}}},\kappa_{l_{\mathrm{c}}}\rangle = |\kappa_{l_{\mathrm{s}}}\rangle\otimes|\kappa_{l_{\mathrm{c}}}\rangle$, is the quasimomentum distribution for the carrier. The asymptotic steady state regime of the motor can be characterized by the dc-component of the averaged velocity; i.e.,

$$v_{\mathrm{c}}(t_0) := \lim_{t\to\infty}\frac{1}{t-t_0}\int_{t_0}^{t} v_{\mathrm{c}}(s;t_0)\,ds \tag{7}$$

Without interaction between the particles, i.e., if $W=0$, for an initially localized carrier with zero velocity *not even a transient directed current does emerge*.[16] This fact holds for *any* shape of the potential $A(t)$. This situation mimics the one taking place in a single-phase, classical ac-motor: a periodically pulsating magnetic field would fail to put a rotor from rest into rotation, unless one applies an initial push via a starter mechanism.[17] Similarly, a single quantum particle when initially localized on a single potential minimum of a periodically modulated ring-shaped potential doesn't acquire any momentum under an unbiased periodic driving force,[16] while a constant bias, $A_B(t) = \omega_B t$, induces Bloch oscillations only.[4] In our setup, it is the ingredient of the interaction with the second particle that takes over the role of a quantum starter.

Notably, even for nonvanishing interaction, i.e., $|W| > 0$, it is still not obvious how to set motor into rotation. Yet again, the seemingly "evident" solution—to apply a constant bias to the carrier—cannot solve the task. Due to the finite coupling with the starter system in

Eq. (3), the corresponding vector potential, $A_B(t) = \omega_B t$, may induce irregular Bloch oscillations with a resulting zero drift velocity only.[18] In distinct contrast, we use here an unbiased time-dependent vector potential possessing a zero dc-component, $\int_0^T A(\tau)\, d\tau = 0$ and being periodic in time, $A(t+T) = A(t)$.

Like for nanomechanical devices,[19] the symmetry principles are of salient importance also for quantum engines: for a zero-momentum initial condition, an ac-force with time-reversal symmetry would launch the system—with equal probabilities—into a clockwise (rightward motion) or a counterclockwise rotation (leftward motion).[20] Taking into account the quantum nature of the engine, the rotor will just spread symmetrically in both direction. Thus, the *modus operandi* requires a symmetry-breaking driving field, realized here with the harmonic mixing signal:

$$A(t) = A_1 \sin(\omega t) + A_2 \sin(2\omega t + \Theta) \tag{8}$$

where Θ denotes the symmetry-breaking phase shift. The input (8) knowingly may induce a non-vanishing nonlinear response, the so-called *ratchet effect*.[20–23]

4. FLOQUET STATES AS TRANSPORT STATES

The dynamics at times $t > t_0$ of the time-periodic Hamiltonian (1) can be analyzed by using the Floquet formalism.[24] The solution of the eigenproblem: $U(t, t_0)|\phi_n(t; k)\rangle = \exp(-(i/\hbar)\epsilon_n(t - t_0))|\phi_n(t; k)\rangle$, with the propagator $U(t, t_0) = \mathcal{T}\exp(-(i/\hbar)\int_{t_0}^{t} H_{\rm tot}(\tau))\, d\tau$ ($\mathcal{T}$ denotes the time ordering), provides the set of time-periodic Floquet states, with $T = 2\pi/\omega$ being the driving period, $|\phi_n(t+T; k)\rangle = |\phi_n(t; k)\rangle$. Here, $k = 2\pi l/L$ with $l = 1, \ldots, L$ is the *total* quasimomentum of the Floquet state. Due to the discrete translation invariance of the system, the total quasimomentum is conserved during the time evolution, thus serving as a quantum number.

In the absence of the driving, $A(t) \equiv 0$, the motor setup (1–3) possesses the continuous translational symmetry in time. In this case, the expansion coefficients of the initial wave-function $\psi(t_0)$ in the system eigenbasis knowingly do not depend on time. On the contrary, eigenstates of a periodically driven system—the Floquet states—evolve in time, being locked by the external ac-field. Thus, the expansion of an initial wave-function over the Floquet eigenbasis depends on the start time t_0 (5), which determines the phase of the driving ac-field,[20] i.e., $|\psi(t_0)\rangle = \sum_{n=1}^{\mathcal{N}} c_n(t_0)|\phi_n(t_0; k)\rangle$, with $c_n(t_0) = \langle\phi_n(t_0; k)|\psi(t_0)\rangle$. Substitution of the above decomposition into (7) yields the result

$$v_c(t_0) = \sum_{n=1}^{\mathcal{N}} \bar{v}_n |c_n(t_0)|^2 \bar{v}_n = \frac{1}{T}\int_{t_0}^{T+t_0} v_n(t)\, dt \tag{9}$$

Here, v_n denotes the velocity expectation value of the n-th Floquet state (6). Because the Floquet states are periodic in time functions, the velocities $\bar{v}_n$ do not depend on t_0, and the dependence of the generated dc-current on the t_0 solely stems from the coefficients $c_n(t_0)$. Since the system evolution is fully quantum coherent; i.e., there is no memory erasing induced by an environment,—the asymptotic current maintains the memory of the initial condition as encoded in the coefficients $c_n(t_0)$.[20]

5. INPUT/OUTPUT CHARACTERISTICS

The question is now, how can we control the motor? To answer this question, we used the symmetry analysis[20] which allows us to predict an appearance of a certain dc current. Combining time-reversal operation and the complex conjugation applied to (1) with $A(t)$ in the form of (8), one can prove the (anti-) symmetric dependence of $\bar{v}_n$ on Θ for the Floquet states with $k = 0$: (i) $\bar{v}_n(-\Theta) = -\bar{v}_n(\Theta)$, and (ii) $\bar{v}_n(\pi - \Theta) = \bar{v}_n(\Theta)$. The first relation implies $\bar{v}_n(0) = -\bar{v}_n(0) = 0$. Then, for $\Theta = 0$, the second relation gives $\bar{v}_n(\pi) = 0$. Thus the Floquet states with $k = 0$ possess zero mean velocities at $\Theta = 0, \pi$. Furthermore, using a similar reasoning, one finds that the set of Floquet states with nonzero k can be ordered by the parity relation, which links eigenstates with opposite quasimomenta, $\phi_n(t; -k; \Theta) = \phi_m(T - t; k; -\Theta)$, yielding $\bar{v}_n(-\Theta) = -\bar{v}_m(\Theta)$. This implies that for a symmetric (in k) initial state and $\Theta = 0, \pi$, the contributions to the dc-current of Floquet states with opposite quasimomenta eliminate each other. The same holds true for a monochromatic driving (8), with $A_2 = 0$.[20] Shifting Θ away from $0, \pm\pi$ causes the decisive symmetry breaking and leads to the desymmetrization of the Floquet states with $k = 0$ and consequently will violate the parity between states with opposite signs of k.

The emergence of a non-vanishing dc current at $\Theta \neq 0, \pi$ induced by the coupling to the starter can be illustrated by the desymmetrization of velocities, $\rho_\kappa(t; t_0)\sin(\kappa + \tilde{A}(t; t_0))$ (as a function of quasimomentum κ), whose sum according to (6) yields the mean velocity of the individual Floquet states. For those with $k = 0$, the desymmetrization happens more drastically since they do not produce any dc current at the symmetry point $\Theta = 0, \pm\pi$. On Figure 2, we depict the instantaneous velocities, $\rho_\kappa(t; t_0)\sin(\kappa + \tilde{A}(t; t_0))$, setting $t_0 = 0$, for a Floquet state with $k = 0$, for $\Theta = 0$, see Figure 2(a), and $\Theta = \pi/2$, see Figure 2(b), together with the resulting mean velocities $v_n(t)$ Figure 2(c). The contributions from different quasimomenta for $\Theta = 0$ eliminate each other and give a periodically varying, but cycle-averaged zero current, see in Figure 2(c), solid line, while the desymmetrization for $\Theta \neq 0$ (b) results in non-vanishing dc current, cf. Figure 2(c), dashed line.

The motor speed depends on the initial conditions, which define the contributions of different Floquet states to the carrier velocity (9). We restrict our analysis to the

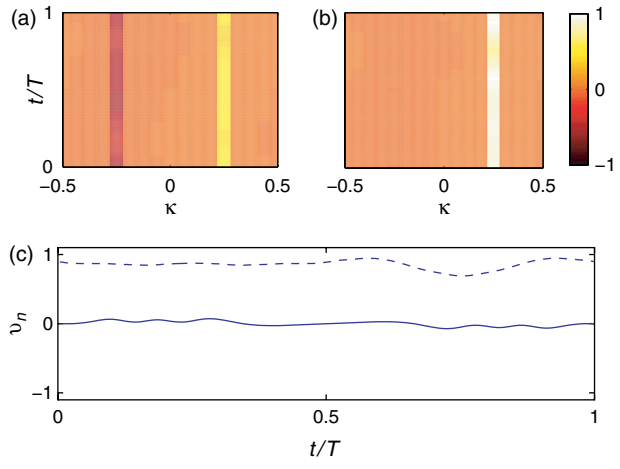

Fig. 2. The colormaps render velocities, $\rho_\kappa(t;t_0)\sin(\kappa+\tilde{A}(t))$, whose sum according to (6) gives the mean velocity of an individual Floquet state with the total quasimomenta $k=0$ for (a) $\theta=0$ and (b) $\theta=\pi/2$, as a function of quasimomentum κ. (c) Velocity of the Floquet states, $\upsilon_n(t)$, for $\theta=0$ (solid line) and $\theta=\pi/2$ (dashed line). Note that while $\upsilon(t)$ for $\Theta=0$ oscillates and is non-zero except few points, its average over period, $\bar{\upsilon}_n$, is strictly zero due to the symmetry $\upsilon_n(t)=-\upsilon_n(T-t)$. The other parameters are $\hbar\omega=0.1\times J_c$, $A_1=0.5$, $A_2=0.25$, $W=0.2J_c$, $J_s=J_c=J$, $L=16$, and $t_0=0$.

initial state $|\psi(t_0)\rangle = L^{-1/2}|l_c\rangle\otimes\sum_{l_s}|l_s\rangle$, $l_c=1,\ldots,L$, in the form of the localized carrier (at l_c) and the uniformly "smeared," delocalized starter. Both particles assume zero velocities at $t=t_0$. The asymptotic velocity may exhibit a strong dependence on t_0.[20] We first discuss the results obtained after averaging over t_0, thus assigning a unique motor velocity value,

$$\upsilon_c = \langle \upsilon_c(t_0)\rangle_{t_0} = \frac{1}{T}\int_{t_0}^{T+t_0} \upsilon_c(t_0)\,dt_0 \qquad (10)$$

for fixed system parameters.

Figure 3 depicts the dependence of the average motor velocity on Θ. The results obtained by direct time propagation of the initial state and averaged over t_0 (dashed line) are superimposed by those calculated via the Floquet formalism (9) (solid line). Both curves show the expected symmetry properties $\upsilon_c(\Theta)=-\upsilon_c(\Theta+\pi)=-\upsilon_c(-\Theta)$. The agreement between the two curves is satisfactory, although not perfect: This is so because the sharp peaks on the asymptotic motor velocity (9) and is due to the finite evolution time used in direct time propagation.

The resonance peaks can be associated with *avoided crossings* between two quasienergy levels (see Fig. 4).[20] These avoided crossings cause a strong velocity enhancement if one of the interacting, and transporting eigenstate overlaps significantly with an initial, non-transporting state of the motor. Note also that a very narrow avoided crossing requires a very large evolution time to become resolved, i.e., $t_{obs}\sim\hbar/|\epsilon_\alpha-\epsilon_\beta|$, see in Ref. [20]. Clearly, our chosen evolution time of 200 T is typically not large enough to clearly resolve the distinct resonances depicted in Figure 2.

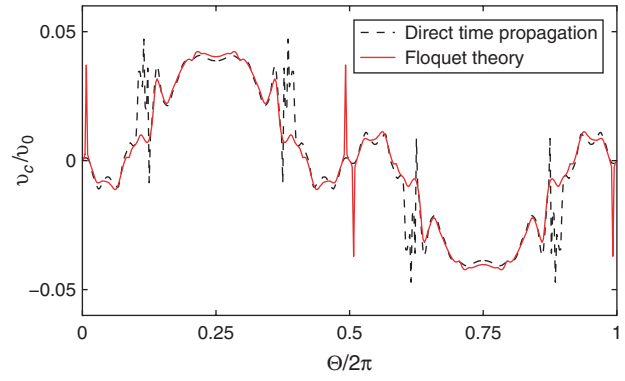

Fig. 3. Averaged motor velocity in (10) (in units of the recoil velocity $\upsilon_0=J_c d/\hbar$) as a function of the phase shift Θ in (8) for $L=16$. The (t_0)-averaged velocity (7) obtained by the direct time propagation of the initial state up to 200 T (dashed line) is compared to the asymptotic dependence given by the Floquet approach (9) (red solid line). Note the anti-symmetry behavior $\upsilon_c(\Theta)=-\upsilon_c(\Theta+\pi)$. The parameters are the same as in Figure 2.

With Figure 4, we show an example of the quasienergy spectrum, $\epsilon_n(\Theta)$, and the carrier and starter velocities, υ_c (solid line) and υ_s (dashed line) respectively, for the coupling constant $W/J=0.01$, and $L=4$. Here we remark that a small coupling constant W yields the avoided crossings smaller while making the resonances sharper. This rather small system size, however, provides already a reasonable number of quasienergies for our elucidation. For every velocity resonance depicted in Figure 4 (bottom), one finds an avoided crossing in Figure 4 (top). The fine avoided crossing structure induces an accompanying fine

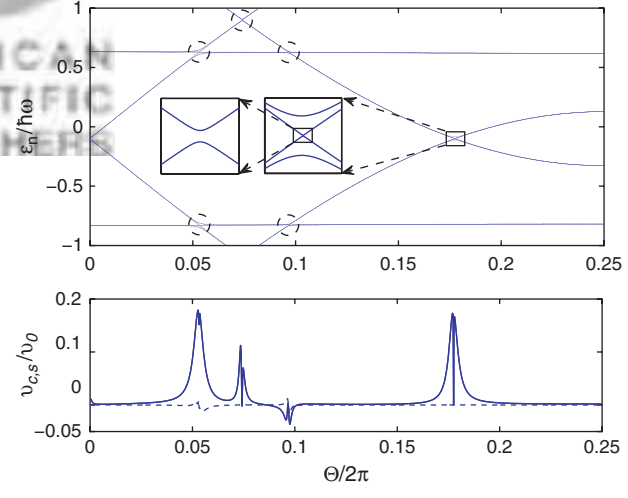

Fig. 4. Resonances of the motor velocity. The quasienergy spectrum (top) and asymptotic carrier/starter velocity (solid/dashed line) in units of $\upsilon_0=J_c d/\hbar$ as a function of θ (bottom), obtained numerically for $\hbar\omega=0.05\times J_c$, $A_1=1$, $A_2=0.5$, $W=0.01\times J_c$, $J_s=J_c$, $L=4$. Presence of the avoided crossings (emphasized by the circles and the rectangle frame) manifests in the resonant velocity peaks at the corresponding values of the phase θ. The insets (top) zoom into the region of one of the avoided crossing: the effect of a tiny anticrossing inside the larger one is clearly resolved in the sharp resonance on top of the wider one (bottom).

structure of corresponding velocity resonances, note the two insets in Figure 4.

So far, we mainly focused on the motor velocity as given by the carrier subsystem velocity. Let us here briefly also comment on the starter dynamics, e.g., a possibly non-zero starter velocity. We found that the averaged starter velocity v_s indeed sensitively depends on the system parameters: It can either be very small compared to the carrier velocity (Fig. 4, bottom, dashed line) or also larger than v_c. In short, the starter can move co-directionally or contra-directionally to the carrier motion.

A robustness of $v_c(t_0)$ against a variation of t_0 characterizes the quality of our quantum motor, as it has been mentioned in the abstract. Looking at the quasimomentum distribution (similar to that of on Figs. 2(a, b)), it becomes evident that ρ_κ weekly depends on time, therefore we could expect that the overlap with the initial state, $c_n(t_0)$, according to (9), and as a result $v_c(t_0)$ has a week dependence on t_0. To provide a more quantitative argument, we calculate the dispersion of the asymptotic motor velocity with respect to the switch on time t_0,

$$\Sigma_v = \sqrt{\langle v_c(t_0)^2 - \langle v_c(t_0)\rangle_{t_0}^2\rangle_{t_0}} \qquad (11)$$

Here we use the direct numerical time-evolution over the sufficiently long time, $t = 500$ T, to approach the asymptotic value (7), see insets in Figure 5. We found that the dispersion becomes increasingly negligible with increasing size L of the lattice. Starting out from $L \gtrsim 16$, the motor gains practically the same asymptotic velocity independently on switch on time t_0.

This effect is due to the presence of the starter: The carrier velocity is obtained as the trace over the part of the total system Hilbert space, $|l_c\rangle \otimes |l_s\rangle$, associated with starter degrees of freedom, $|l_s\rangle$. The starter dynamics mimics a finite "heat bath" for the carrier dynamics whose effectiveness increases with both, the (i) the dimension of the starter subspace, i.e., the size L, and (ii) the strength of the interaction W.

6. LOAD CHARACTERISTICS

Thus far, the analysis of the system in Eqs. (1)–(3), (8) has been performed in a idle-running mode with no load applied. In order to qualify for a genuine motor device, the engine must be able to operate under an applied load. The load is introduced in the form of an additional bias $A_B(t) = \omega_B t$, being added to the vector potential $\tilde{A}(t)$. All the information about transport properties can be extracted by using again the Floquet formalism, provided that the ac-driving and the Bloch frequencies are mutually in resonance;[26] i.e., we have the condition $q \cdot \omega = r \cdot \omega_B$ obeyed, where r and q are co-prime integers. Figure 6 depicts the range of velocity values for Floquet eigenbasis, $\bar{v}_n$, see part (a), and the dependence of the resulting asymptotic motor speed, v_c, for different bias values, part (b). There occur two remarkable features. First, the spectrum of velocities is symmetric around $\omega_B = 0$. This follows because of the specific choice of the phase shift at $\Theta = \pi/2$. Second, while some regimes provide a transport velocity along the bias, others correspond to the up-hill motion, against the bias. Therefore, a stationary transport in either direction is feasible. The load characteristics

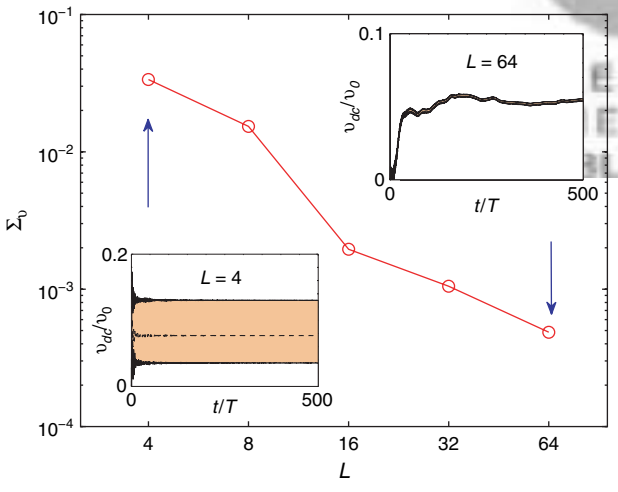

Fig. 5. Dispersion of the motor velocity (11) versus the number of lattice sites L. The dependence of the asymptotic direct current on t_0 vanishes with increase of the lattice size. The insets show the running average for the carrier velocity. For both insets two realizations of t_0, which give the maximal and minimal values of the asymptotic velocity are depicted (solid lines), with remaining realizations for different t_0 varying in between these lines. The dependence averaged over 20 realizations is depicted in both insets by a dashed line. Note that for $L = 64$ the range bounded by two curves practically shrinks to the single thick line. Here $\theta = \pi/2$, and the other parameters are the same as in Figure 2.

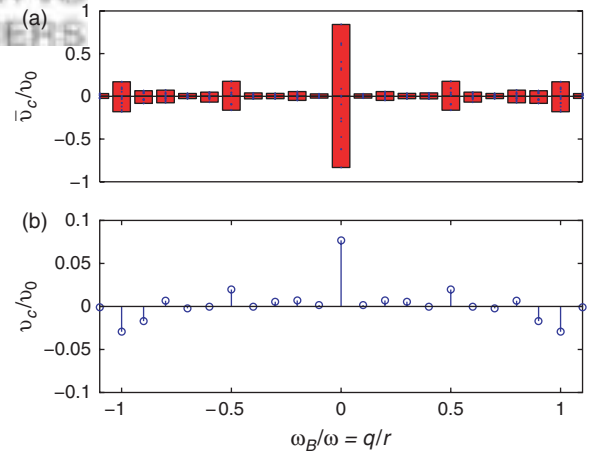

Fig. 6. Average motor velocity versus the load $A_B(t) = \omega_B t$. (a) The range of velocity values for the Floquet eigenbasis. (b) The average motor velocity for the initial condition with the localized carrier and the delocalized starter. We set $\omega_B = \omega \cdot q/r$, with $r = 10$, and vary the integer q. The parameters are $W = 0.2J_c$, $J_s = J_c = J$, $\hbar\omega = 0.1J_c$, $A_1 = 0.5$, $A_2 = 0.25$, $\Theta = \pi/2$, and $L = 4$.

exhibits a discontinuous, fractal structure. In distinct contrast to the classical case,[27,28] it cannot be approximated by a smooth curve. This is a direct consequence of the above mentioned resonance condition.

7. EXPERIMENTAL REALIZATIONS

We next discuss the parameter range where the carrier atom generates a tangible dc current. In the fast-driving limit, $\omega \gg W/(\hbar(|A_1|+|A_2|))$, the Floquet states adiabatically follow the instantaneous eigenstates of the total Hamiltonian in presence of (1) *zero particle-interaction* i.e., $W = 0$. Thus, the resulting, fast driven dc current approaches zero. In the slow-driving limit, $\omega \ll W/(\hbar(|A_1|+|A_2|))$, the Floquet states adiabatically follow the associated instantaneous levels of the static Hamiltonian (1) with no dynamical symmetry-breaking field acting; thus the slow-driven dc current vanishes as well. Thus the maximum dc current region is located in the intermediate region, $\omega \sim W/(\hbar(|A_1|+|A_2|))$.

For an experimental realization of this quantum atom motor the following feature should be respected: Because in the tight-binding approximation the maximal amplitude of the tunneling is limited from above, $J_c \lesssim J_{max} = 0.13E_0$, for, e.g., a ^{6}Li "carrier," a lattice constant $d \sim 10\ \mu$m, and with $\hbar\omega = 0.1J_c$ as used in the present calculations, the driving frequency ω should be less than 2 Hz. Then, the time required to launch the motor; i.e., for it to approach the asymptotic velocity, which is $\sim 0.05v_0 \approx 30\ \mu$m/s $\approx$ 3 sites/second, is around a minute. Further focusing of the laser beam can decrease the lattice constant d, thereby decreasing the launch time to experimentally accessible coherence times around 10 seconds[29] and increasing the asymptotic velocity.

8. CONCLUSIONS

We elaborated in greater detail on the working principles of the quantum electric ac-motor that is made of two ultracold interacting atoms only:[12] a carrier and a starter, moving in a optical bracelet potential. The central result of this study is an evident directed coherent carrier motion that is induced by the starting mechanism. The emerging motor velocity can suitably be controlled by means of the symmetry breaking, time-dependent, bichromatic, external magnetic flux. Importantly, for zero-momentum initial conditions the asymptotic carrier velocity loses its dependence on the switch-on time t_0 of the ac-drive upon increasing the bracelet size L.

An extension of our motor setup to several interacting carries or starters (i.e., multiple rotor motors or finite bosonic "heat baths") presents an intriguing challenge. A particular interesting objective to pursue is the problem of whether the motor velocity can be optimally tuned with the number of participating atoms?

Finally, an exciting perspective is to physically couple our quantum motor to a nano-mechanical resonator.[30] Such a hybrid system can be used to power quantum mechanically such a classical object.

This work was supported by the DFG through grant HA1517/31-1 and by the German Excellence Initiative "Nanosystems Initiative Munich (NIM)."

References

1. H. J. Metcalf and P. van der Straten, Laser Cooling and Trapping, Springer, New York, USA **(2007)**.
2. M. H. Anderson, J. R. Ensher, M. R. Matthews, C. E. Wieman, and E. A. Cornell, *Science* 269, 198 **(1995)**; K. B. Davis, M. O. Mewes, M. R. Andrews, N. J. van Drutten, D. S. Durfee, D. M. Kurn, and W. Ketterle, *Phys. Rev. Lett.* 75, 3969 **(1995)**.
3. R. Feynman, *Int. J. Theor. Phys.* 21, 467 **(1982)**.
4. O. Morsch and M. Oberthaler, *Rev. Mod. Phys.* 78, 179 **(2006)**.
5. D. Schrader, I. Dotsenko, M. Khudaverdyan, Y. Miroshnychenko, A. Rauschenbeutel, and D. Meschede, *Phys. Rev. Lett.* 93, 150501 **(2004)**.
6. T. Akatsuka, M. Takamoto, and H. Katori, *Nature Phys.* 4, 954 **(2008)**.
7. A. D. Cronin, J. Schmiedmayer, and D. E. Pritchard, *Rev. Mod. Phys.* 81, 1051 **(2009)**.
8. B. Canuel, F. Leduc, D. Holleville, A. Gauguet, J. Fils, A. Virdis, A. Clairon, N. Dimarcq, Ch. J. Borde, and P. Bouyer, *Phys. Rev. Lett.* 97, 010402 **(2006)**.
9. The conversion of electrical energy into mechanical work by electromagnetic means was devised by Michael Faraday in 1821. The first operating electric motor was demonstrated by Ányos Jedlik in 1828.
10. J. G. Korvink and O. Paul, Microelectromechanical Systems: A Practical Guide to Design, Analysis, and Applications, Springer, Norwich, New-York **(2006)**.
11. A. M. Fennimore, T. D. Yuzvinsky, W.-Q. Han, M. S. Fuhrer, J. Cumings, and A. Zettl, *Nature* 424, 408 **(2003)**; D. L. Fan, F. Q. Zhu, R. C. Cammarata, and C. L. Chien, *Phys. Rev. Lett.* 94, 247208 **(2005)**; B. C. Regan, S. Aloni, K. Jensen, R. O. Ritchie, and A. Zettl, *Nano Lett.* 5, 1730 **(2005)**.
12. A. V. Ponomarev, S. Denisov, and P. Hänggi, *Phys. Rev. Lett.* 102, 230601 **(2009)**.
13. L. Amico, A. Osterloh, and F. Cataliotti, *Phys. Rev. Lett.* 95, 063201 **(2005)**.
14. S. Franke-Arnold, J. Leach, M. J. Padgett, V. E. Lembessis, D. Ellinas, A. J. Wright, J. M. Girkin, P. Ohberg, and A. S. Arnold, *Opt. Exp.* 15, 8619 **(2007)**.
15. S. Viefers, P. Koskinen, P. Singha Deo, and M. Manninen, *Phys. E* 21, 1 **(2004)**.
16. I. Goychuk and P. Hänggi, *J. Phys. Chem. B* 105, 6642 **(2001)**.
17. A. Hughes, Electric Motors and Drives, 3rd edn., Newnes, London **(2006)**.
18. A. V. Ponomarev, J. Madronero, A. R. Kolovsky, and A. Buchleitner, *Phys. Rev. Lett.* 96, 050404 **(2006)**.
19. W. K. Liu, E. G. Karpov, and H. S. Park, Nanomechanics and Materials: Theory, Multiscale Methods and Applications, Wiley, Chichester, West Sussex, UK **(2006)**.
20. S. Denisov, L. Morales-Molina, S. Flach, and P. Hänggi, *Phys. Rev. A* 75, 063424 **(2007)**.
21. P. Hänggi and F. Marchesoni, *Rev. Mod. Phys.* 81, 387 **(2009)**.
22. M. Schiavoni, L. Sanchez-Palencia, F. Renzoni, and G. Grynberg, *Phys. Rev. Lett.* 90, 094101 **(2003)**; P. H. Jones, M. Goonasekera, and F. Renzoni, *Phys. Rev. Lett.* 93, 073904 **(2004)**; R. Gommers, S. Bergamini, and F. Renzoni, *Phys. Rev. Lett.* 95, 073003 **(2005)**.

23. I. Goychuk and P. Hänggi, *Europhys. Lett.* 43, 503 **(1998)**.
24. M. Grifoni and P. Hänggi, *Phys. Rep.* 304, 229 (**1998**).
25. S. Kohler, J. Lehmann, and P. Hänggi, *Phys. Rep.* 406, 379 **(2005)**.
26. M. Glück, A. R. Kolovsky, and H. J. Korsch, *Phys. Rep.* 366, 103 **(2002)**.
27. M. Kostur, L. Machura, P. Hänggi, J. Luczka, and P. Talkner, Physica A 371, 20 (**2006**).
28. M. Kostur, L. Machura, P. Talkner, P. Hänggi, and J. Luczka, *Phys. Rev. B* 77, 104509 (**2008**).
29. M. Gustavsson, E. Haller, M. J. Mark, J. G. Danzl, G. Rojas-Kopeinig, and H.-C. Nägerl, *Phys. Rev. Lett.* 100, 080404 **(2008)**.
30. K. L. Ekinci and M. L. Roukes, *Rev. Sci. Instrum.* 76, 061101 **(2005)**.

Received: 18 October 2009. Accepted: 1 November 2009.